Supporting Information for:

A Photoactivatable Upconverting Nanodevice Boosts Lysosomal Escape of PROTAC Degraders for Enhanced Combination Therapy

Jiayin Zhan,[#a] Xiang Li,[#a] Yueru Mu,[a] Huiqin Yao,[b] Jun-Jie Zhu*[a] and Jingjing Zhang*[a,c]

[a.] State Key Laboratory of Analytical Chemistry for Life Science, School of Chemistry and Chemical Engineering, Nanjing University, Nanjing 210023, China.

[b.] Department of Medical Chemistry, College of Basic Medicine, Ningxia Medical University, Yinchuan 750004, China.

[c.] Chemistry and Biomedicine Innovation Center (ChemBIC), Nanjing University, Nanjing 210023, China.

*Email: yaohq@nxmu.edu.cn; jjzhu@nju.edu.cn; jing15209791@nju.edu.cn.

Table of Contents

Section A: Reagents and apparatus

Reagents

High sensitive ECL luminescence reagent (C500044) and Cell Counting Kit-8 (CCK-8, E606335) were provided by Shanghai Sangon Biological Engineering Co., Ltd. (Shanghai, China). Hoechst 33342 and Acridine Orange Staining Kit were obtained from Beyotime Biotechnology Co., Ltd. (Shanghai, China). Sodium hydroxide (NaOH, 98%), yttrim (III) chloride hexahydrate (YCl_3•$6H_2O$, 99.99%), ytterbium (III) chloride hexahydrate ($YbCl_3$•$6H_2O$, 99.99%), erbium (III) chloride hexahydrate ($ErCl_3$•$6H_2O$, 99.99%) were purchased from Aladdin Co., Ltd. (Shanghai, China). Oleic acid (OA, 90%) and 1-octadecene (ODE, 90%) were obtained from Alfa Aesar. Ammonium fluoride (NH_4F, 99.9%) and poly-(L-lysine) were purchased from Macklin Co., Ltd. (Shanghai, China). Dulbecco's modified Eagle's medium (DMEM), phosphate buffered saline (1×PBS) (10mM, pH 7.4), DCFH-DA were bought from Keygen Biotech (Nanjing, China). The MCF-7 cells used in this study were obtained from ATCC. All solutions were prepared with Millipore water (18.25 $M\Omega \cdot cm^{-1}$). All animal experiments were approved by the Institutional Animal Care and Use Committee (IACUC) of Nanjing University (Approval No: IACUC-2312005). 6-8 week-old nude mice (female) were provided by Gempharmatech Co., Ltd. Live & Dead™ Viability/ Cytotoxicity Assay Kit for Animal Cells (Calcein AM, PI) (L6037S, UElandy, Suzhou, China) according to the protocol provided by the manufacturer. Annexin V-FITC/PI Apoptosis Detection Kit (A211-01) were purchased from Vazyme Biotech Co., Ltd. (Nanjing, China). Western blots were performed with antibodies against of BRD4 (28486-1-AP, Proteintech, 1:2000), c-Myc (10828-1-AP, Proteintech, 1:5000), Caspase 3/Cleaved Caspase 3 (19677-1-AP, Proteintech, 1:1000), β-actin (D6A8, Cell Signaling Tech., 1:1000) and anti-rabbit IgG, HRP-conjugated secondary antibody (#7074, Cell Signaling Tech., 1:1500). MLN4924 (S81085) was purchased from Yuanye Bio-Technology Co., Ltd. (Shangghai, China). MG132 (Cat# 2194) was from Cell Signaling Tech. LysoTracker Green DND-26 (40738ES) was obteined from Yeasen Biotechnology Co., Ltd. (Shanghai, China). dBET6 (HY-112588) was purchased from MedChemExpress (MCE, USA).

Apparatus

The fluorescence emission spectra of DCFH-DA were recorded on a F-320 fluorimeter (Gangdong Sci.&Tech. Development Co. Ltd., China). The fluorescence spectra of UCNPs were collected on FLS980 fluorescence spectrometer (Edinburgh, UK) with a continuous-wave laser (980 nm) as the excitation light. The transmission electron microscopic (TEM) images were obtained using a JEM-2800 (200 kV) (JEOL Co., Ltd., Japan). The high-resolution transmission electron microscopy (HRTEM) , high-angle annular dark-field scanning transmission electron microscopy (HAADF-STEM) characterization and corresponding Energy Dispersive Spectrometer (EDS) mapping were performed on a Talos F200S (FEI, USA). The gel electrophoresis was operated on EPS-600 electrophoresis apparatus. Fourier-transform infrared (FTIR) spectra were obtained on Nicolet iS50 (Thermo, USA). Zeta potential analysis was conducted on 90Plus Zeta (Brook haven, USA). The cytotoxicity assays were performed on a Synergy H1 Multi-Mode Microplate Reader (Bio-Tek Instrument, USA). X-ray diffraction (XRD) measurement was conducted on a Thermo ARL SCINTAG X'TRA diffractometer using a Cu-Kα radiation (λ = 0.15405 nm). Cell images were obtained on a Sp8 confocal laser scanning microscope (CLSM) (Leica, Germany). Flow cytometric analysis of cells was conducted using a CytoFlex flow cytometry system (Beckman Coulter Inc., USA). *In vivo* fluorescence images were acquired and analysed using the IVIS Lumina XR III *in vivo* imaging system (PerkinElmer, USA). The UV-visible absorption spectra was measured using UV-8000 (Metash, China). Nitrogen adsorption/desorption measurements were conducted on ASAP 2460 (Micromeritics, USA). High-performance liquid chromatography (HPLC) was carried out on Thermo Scientific Dionex Ultimate 3000 with CH_3CN/H_2O (1‰ TFA) as eluents (mobile phase: A: CH_3CN with 0.1% TFA; B: H_2O with 0.1% TFA; flow rate: 1 mL/min; column temperature: 25 °C; UV: 254 nm; elute gradient: 0 - 30 min, from 10% A to 95% A).

Section B: Experimental details

B1. Preparation and characterization of the DNA nanomachine

B1.1 Synthesis of $NaYF_4$:Yb,Er UCNPs.

The monodispersed UCNPs was prepared in a three-necked flask under magnetic stirring by adding 0.78 mmol of YCl_3•$6H_2O$, 0.2 mmol of $YbCl_3$•$6H_2O$ and 0.02 mmol of $ErCl_3$•$6H_2O$ into the mixture of 6 mL of OA and 15 mL of ODE and then heating to 150 °C under nitrogen protection for 60 min. After cooling down to the room temperature, 100 mg of NaOH and 150 mg of NH_4F were dissolved in 5 mL of methanol and were added into the rare-earth salt solution. After vigorously stirring for 60 min, the reaction temperature was first increased to 80 °C to remove methanol and then increased to 120 °C for 10 min. Subsequently, the solution was heated to 300 °C for 60 min under nitrogen protection to form $NaYF_4$:Yb,Er. After the mixture was cooled, the UCNPs were precipitated by adding excessive ethanol and were purified by centrifugation and dispersed in the cyclohexane for further use.

B1.2 Synthesis of RB-HA.

RB (1 g) and 6-bromohexanoic acid (0.6 g) were dissolved in 6 mL of DMF and the mixture was heated to 80 °C for 7 h. After the reaction was completed, the product was cooled naturally to room temperature, and the excess DMF was removed via rotary evaporation. Then excessive ether (30 mL) was added to the solid product and the mixture was stirred overnight. The product was obtained by centrifugation at 4000 rpm for 5 min. After that, 30 mL of water was added to the solid and stirred for 12 h. After stirring, vacuum suction filtration was operated, and the product was collected and dried. Next, the solid product was dissolved in a small amount of ethanol (10 mL), and then recrystallized at 4 °C. Finally, RB-HA was purified via rotary evaporation to remove ethanol, and the final product was collected for further reaction.

B1.3 Synthesis of RB-NHS.

The as-synthesized RB-HA (457 mg), NHS (193.4 mg) and EDC·HCL (241.5 mg) were dissolved in 3.5 mL of DMF in a flask and the mixture was stirred overnight. Afterwards, the DMF was removed via rotary evaporation. The product was extracted with water and chloroform, and was transferred into chloroform below. The chloroform was removed by spin evaporation, and the solid product was stirred with 30 mL of ether overnight. Finally, RB-NHS was collected by and filtered by vacuum suction filtration.

B1.4 Loading content of dBET6 on USNs.

To obtained the standard curve, HPLC was carried out to measure the absorbance peak area at the 254 nm at concentrations of 0.5, 2, 5, 10 and 20 μM. The obtained data could facilitate the determination of the linear standard curve after linear fitting. Then, 0.5 mL USNs (4 mg/mL) were dispersed in excess dBET6/DMSO solutions and stirred overnight at room temperature. The complexes were centrifuged and washed several times. Subsequently, the concentration of dBET6 remained in the supernatants was examined by HPLC and was calculated with the linear standard curve (Peak area=2.4522*C-2.6889). The loading content of dBET6 on USNs was calculated to be 10 nmol/mg.

B2. Evaluation of the USDPR nanodevice in living cells

B2.1 Cell culture.

MCF-7 cells were utilized in the experiments and were cultured in DMEM medium complemented with 10% fetal bovine serum (FBS), 100 U/mL penicillin, and 100 μg/mL streptomycin in an incubator containing 5% CO_2 at 37 °C.

B2.2 Cytotoxicity assay.

1×10^4 MCF-7 cells were seeded in 96-well plate and incubated until 60-70% confluence. For time-dependent investigation, the cell viability of MCF-7 cells under different treatments were tested during different time periods, such as 0 h, 6 h, 12 h, 24 h, 48 h. For dose-dependent investigation, MCF-7 cells were treated with a series concentrations of different nanodevices at 37 °C, and excess nanoparticles were washed away by PBS after 6-hour-incubation. Afterwards, cells in fresh DMEM medium were irradiated with 980 nm NIR light for 4 min (2 W/cm^2, 1 min break after 2 min irradiation). At the end of the treatment period, the cell viability was detected with CCK-8 assay kit according to the manufacturer's instruction.

B2.3 Cell apoptosis analysis by flow cytometry.

5×10^5 MCF-7 cells were seeded in 12-well plates and incubated until 70-80% confluency. Then, cells were treated with DMEM containing different nanoparticles, including USD, USPR, and USDPR (90 μg/mL) for 6 h. After being washed three times with PBS to remove the uninternalized nanoparticles, the cells were treated with or without 980 nm NIR irradiation as indicated (2 W/cm^2 for 4 min, 1 min break after 2 min irradiation). Untreated cells were used as negative control. After 24 h culturation, the cells were washed thoroughly with PBS and stained using Annexin V-FITC/PI Apoptosis Detection Kit under light-proof conditions. Subsequently, the apoptosis was quantitatively assessed by flow cytometric analysis. Flow cytometry measurements were made with n = 5000 events and performed in triplicates at the minimum.

B3. Evaluation of the DNA nanomachine in living mice

B3.1 Animal model.

All animal experiments in this work were approved by the IACUC of Nanjing University (**Approval No: IACUC-2312005**). 6-8 week-old BALB/c nude mice (female) were provided by Gempharmatech Co., Ltd. To establish the subcutaneous MCF-7 tumor model, 5×10^6 MCF-7 cells were injected into the right lower flank of the female BALB/c nude mice. *In vivo* experiments were further carried out until the tumor volume reached approximately 60 mm^3. The tumor volume (V) was calculated via the following equation: $V = 0.5 \times (\text{Length} \times \text{Width}^2)$.

B3.2 Fluorescence imaging of ROS *in vivo*.

For the detection of *in vivo* ROS production, the mice were treated similarly to group USDPR and intratumorally injected with 50 μL of 2 mM DCFH-DA before NIR irradiation. As a negative control, the tumor was injected with USDPR (2 mg/kg) and DCFH-DA without NIR irradiation. The fluorescence images of mice were captured before and after NIR irradiation (2 W/cm^2 for 4 min, 1 min break after 2 min irradiation). A 520 nm filter was used to measure the fluorescence signal emitted from the oxidation of DCFH-DA. Then, the mice were euthanized and the treated tumors were harvested and evaluated using IVIS Spectrum, followed by frozen and sliced up. Before CLSM imaging, the sections were stained by DAPI.

B3.3 Histology.

At the end of the treatment, the mice were euthanized and dissected, and the tumors and main organs (heart, liver, spleen, lung and kidney) were excised for further hematoxylin-eosin (H&E) staining. The therapeutic efficacy was assessed by Ki67 immunofluorescence staining and terminal deoxynucleotidyl transferase (TdT)-mediated deoxyuridine triphosphate (dUTP) nick end labeling (TUNEL) assays. BRD4 and c-Myc immunofluorescence analysis and western blotting were carried out to investigate the BRD4 protein levels in tumors. The tissue sections were prepared by the Servicebio Biotech Company (Wuhan, China) for histopathology evaluation.

Section C: Supporting Figures

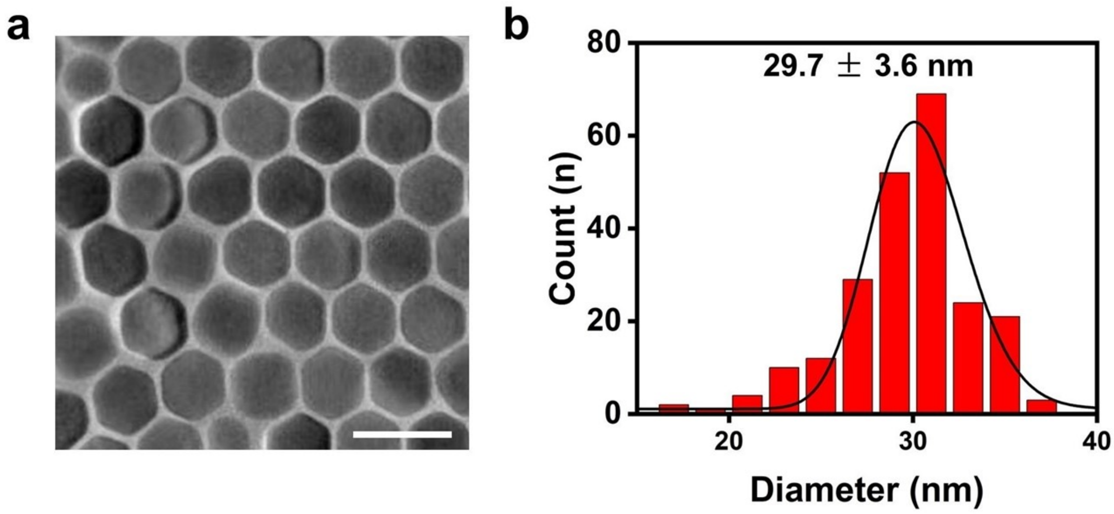

Figure S1. (a) TEM image of UCNPs. Scale bar: 50 nm. (b) Size distribution of UCNPs.

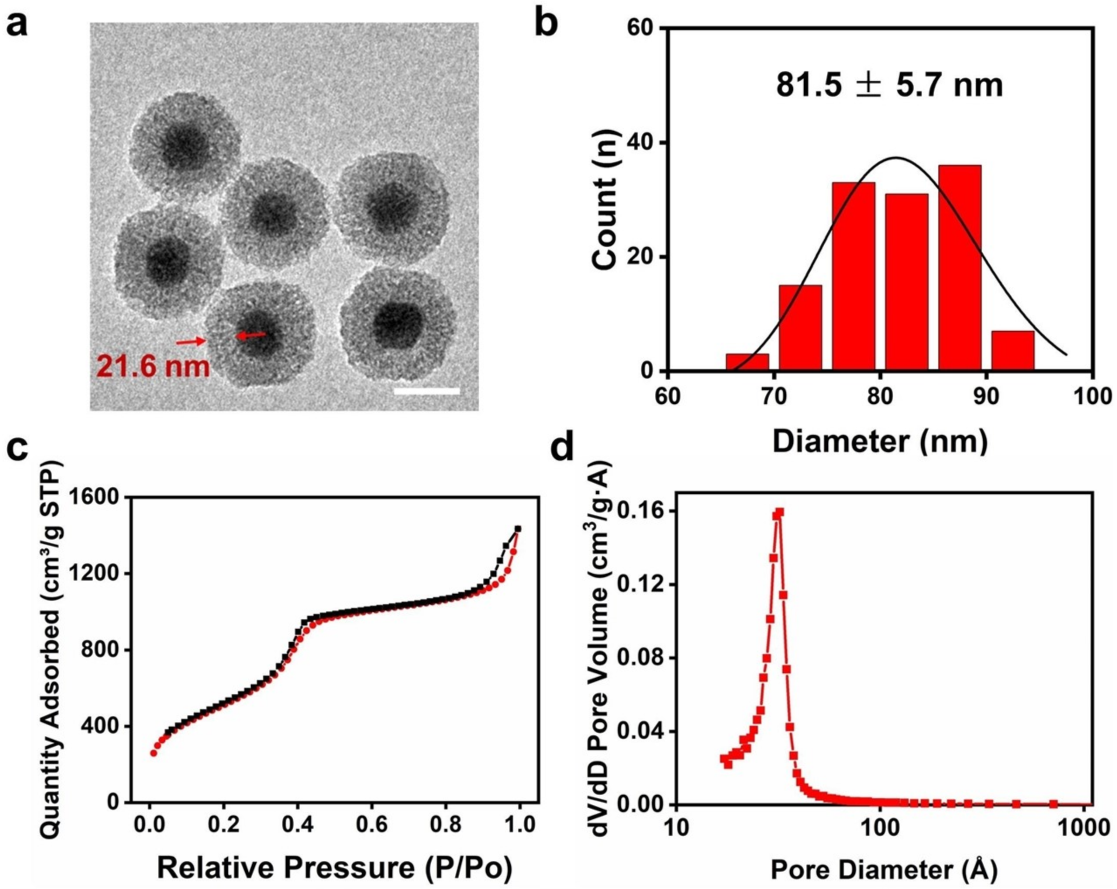

Figure S2. (a) TEM image of USN (scale bar: 50 nm). (b) Size distribution of USN. (c) N_2 adsorption/desorption isotherm of USN. (d) The pore-size distribution plot of USN obtained from BET adsorption isotherm experiments.

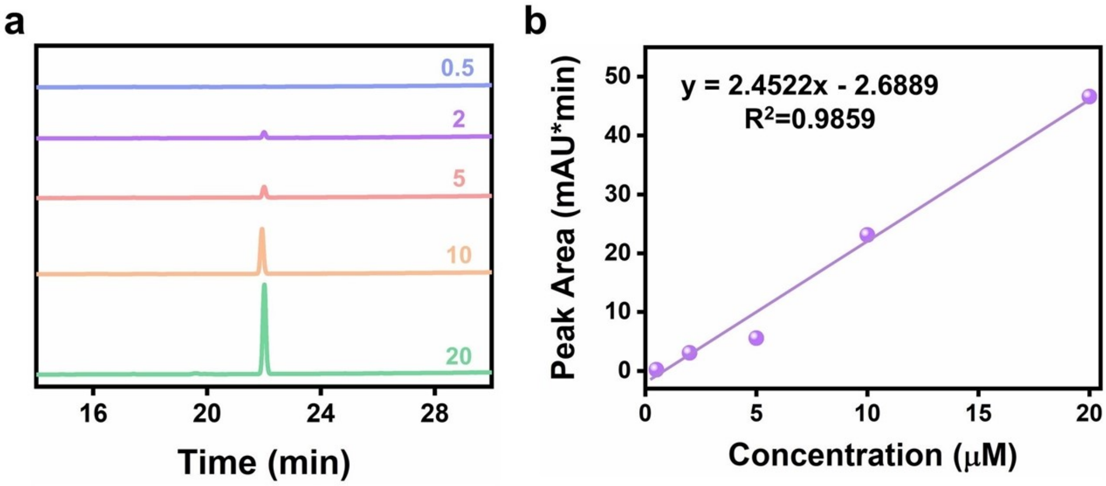

Figure S3. (a) HPLC analysis of different concentrations of dBET6 (0.5, 2, 5, 10, 20 μM). (b) The standard curve of dBET6 quantified by HPLC analysis in (a).

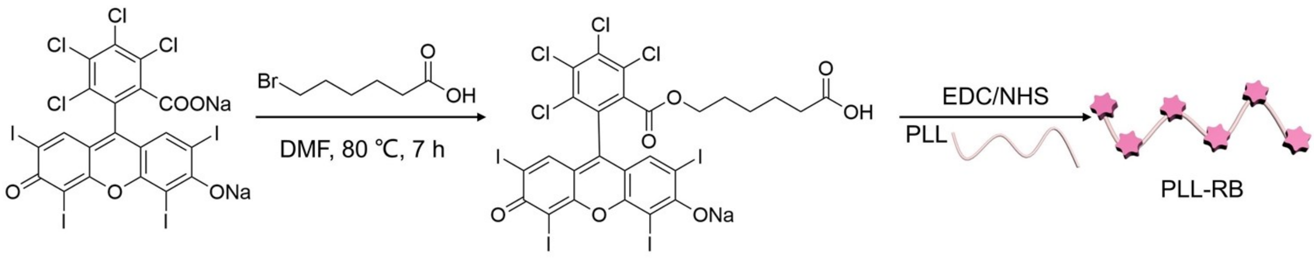

Figure S4. Schematic diagram for the synthetic pathway of PLL-RB.

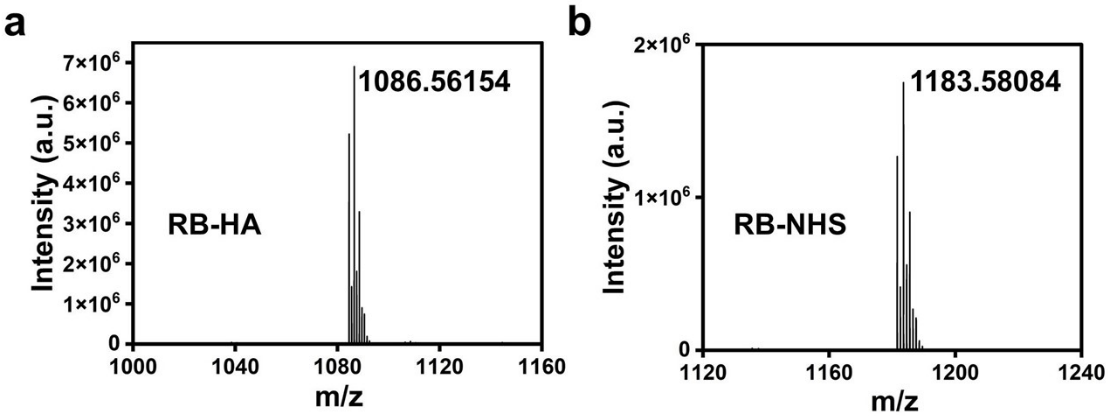

Figure S5. Electrospray ionization-high resolution mass spectrometry (ESI-HR MS) of compound (a) RB-HA (calculated molecular weight: 1086.56, measured: 1086.56154) and (b) RB-NHS (calculated molecular weight: 1183.58, measured: 1183.58084).

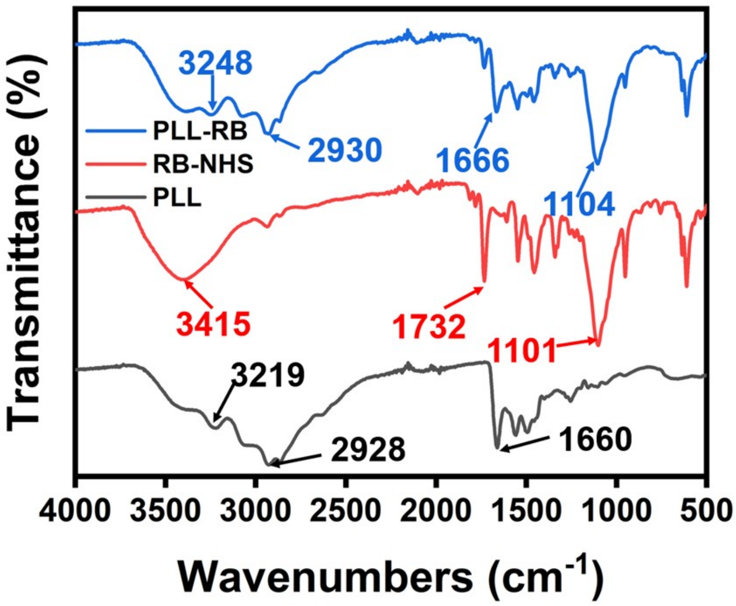

Figure S6. FTIR spectra of PLL (black curve), RB-NHS (red curve), and PLL-RB (blue curve). For PLL, the band at 2928 cm^{-1} was attributed to the antisymmetric stretching of $-CH_2$ in PLL. The band at 3219 cm^{-1} referred to the N-H stretching vibrations and the band at 1660 cm^{-1} referred to the stretching vibrations of C=O bonds. For RB-NHS, the band at 3415 cm^{-1} referred to the O-H stretching vibrations and the band at 1732 cm^{-1} referred to the stretching vibrations of C=O bonds. The band at 1101 cm^{-1} was attributed to the C-O-C stretching vibrations. For PLL-RB, the band at 3248 cm^{-1} referred to the O-H stretching vibrations and the band at 2930 cm^{-1} referred to the stretching vibrations of C-H bonds. The band at 1666 cm^{-1} was attributed to the C=O stretching vibrations and the band at 1104 cm^{-1} was attributed to the C-O-C stretching vibrations. These characteristic FTIR peaks of PLL and RB verified the successful crosslinking through the covalent bonds.

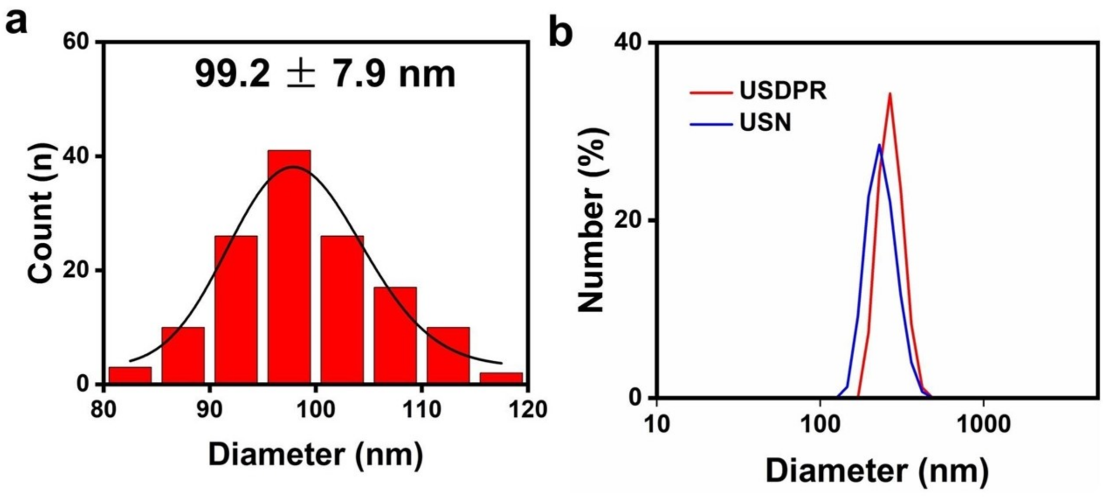

Figure S7. (a) Size distribution of USDPR. (b) Dynamic light scattering (DLS) analysis of hydrodynamic size distribution of USN and USDPR.

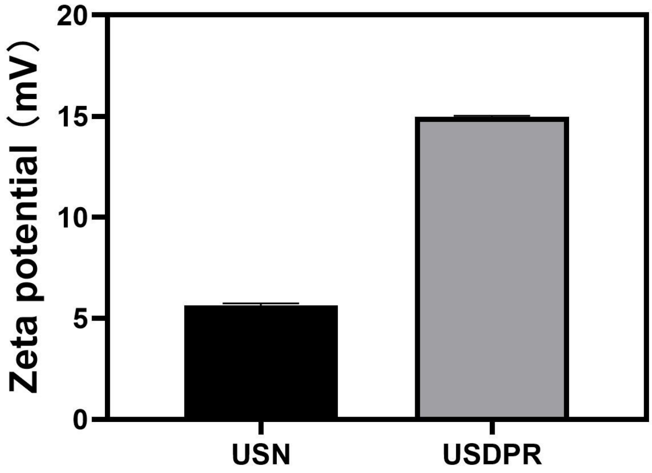

Figure S8. Zeta potentials analysis of USN and USDPR. Error bars represent the standard deviations of three independent experiments.

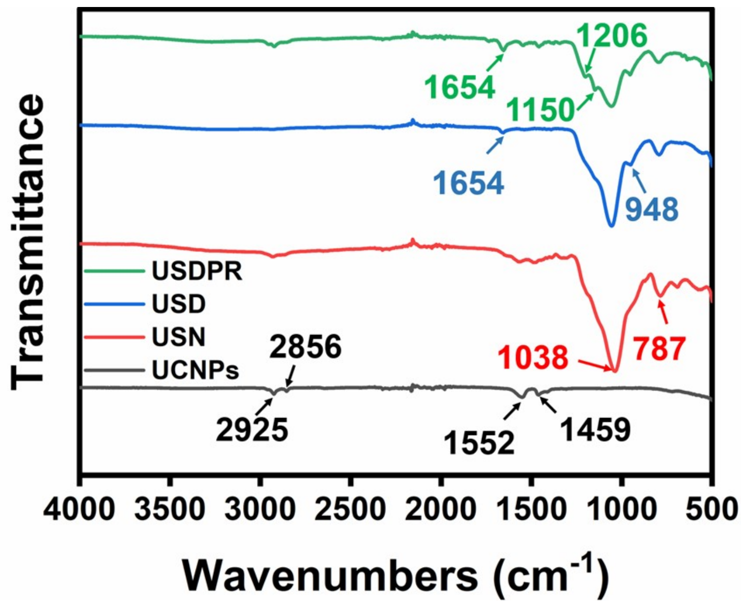

Figure S9. FTIR spectra of UCNPs (black curve), USN (red curve), USD (blue curve), and USDPR (green curve).

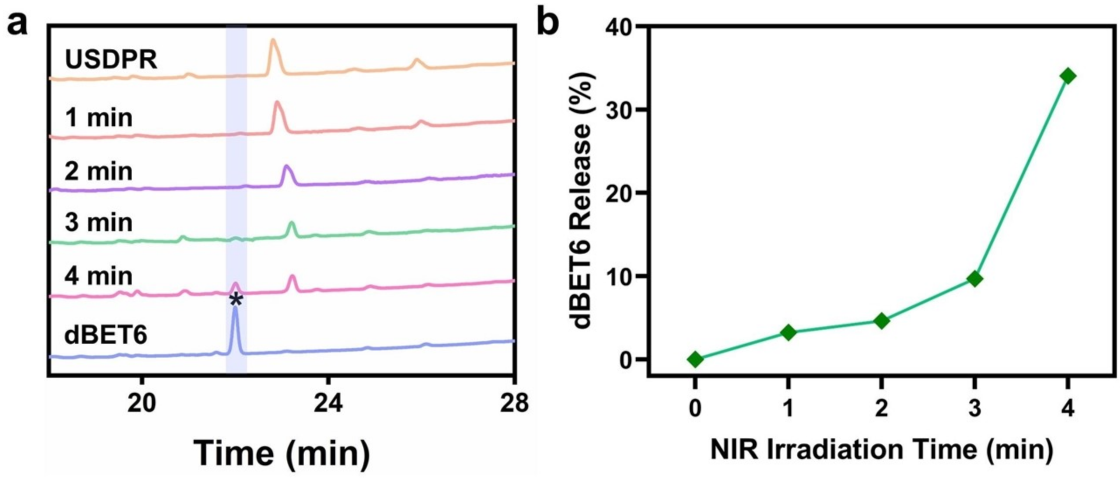

Figure S10. (a) HPLC profiles of dBET6 released from USDPR with 980 nm NIR irradiation for different times (0-4 min). (b) Quantification of the proportion of the released dBET6 based on the peak area at 22-min-retention time in (a).

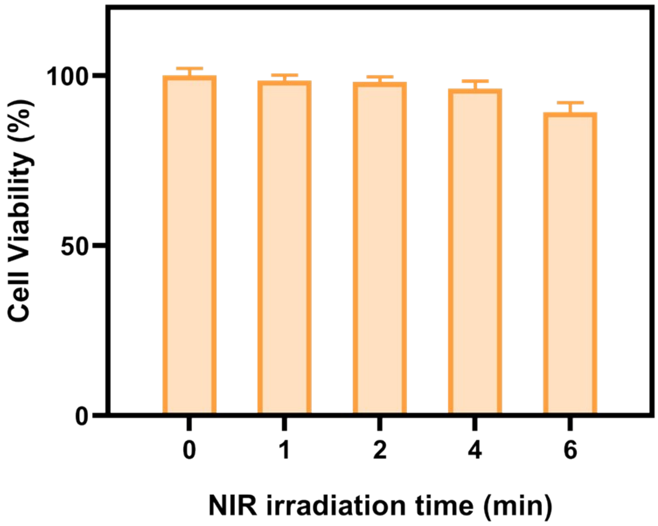

Figure S11. Cell viabilities of MCF-7 cells treated with 980 nm NIR irradiation for different time and further cultured for 24 h. Data are the mean ± SD (n = 3).

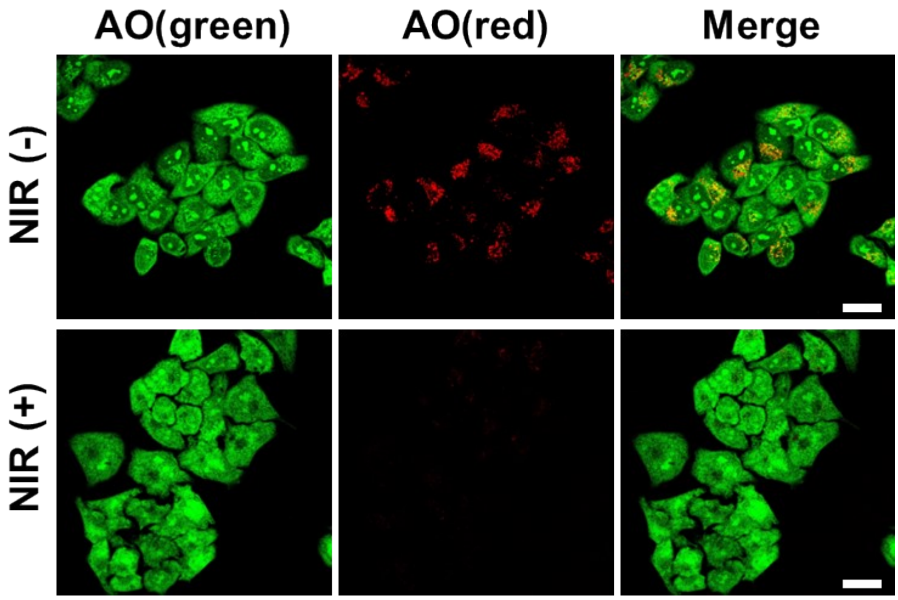

Figure S12. Confocal fluorescence images of MCF-7 cells incubated with AO to evaluate endosomal integrity after the treatment with USDPR with or without 980-nm NIR irradiation. Scale bar: 20 μm.

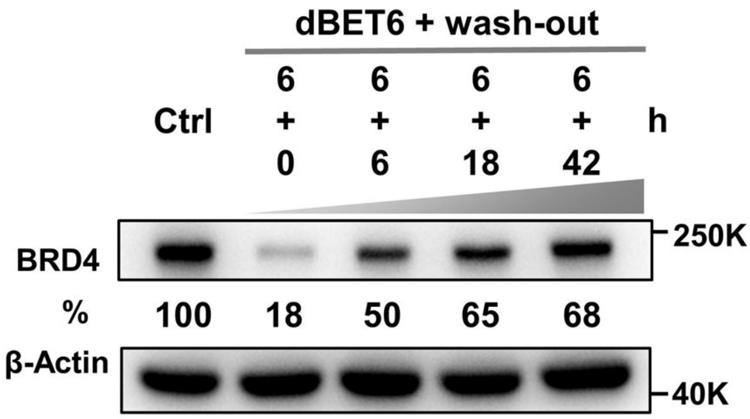

Figure S13. Western blot analysis of BRD4 protein levels in MCF-7 cells treated with free dBET6 for 6 h and further cultured for different time periods after wash-out.

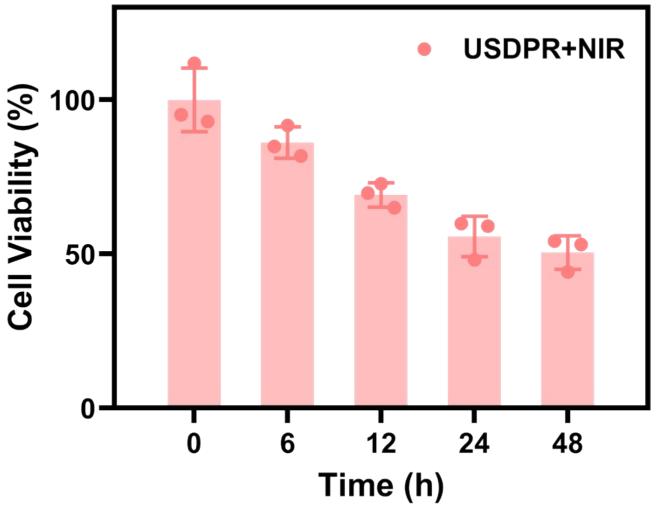

Figure S14. Cell viabilities of MCF-7 cells treated with USDPR and 980 nm NIR irradiation during different time periods. Data are the mean ± SD (n = 3).

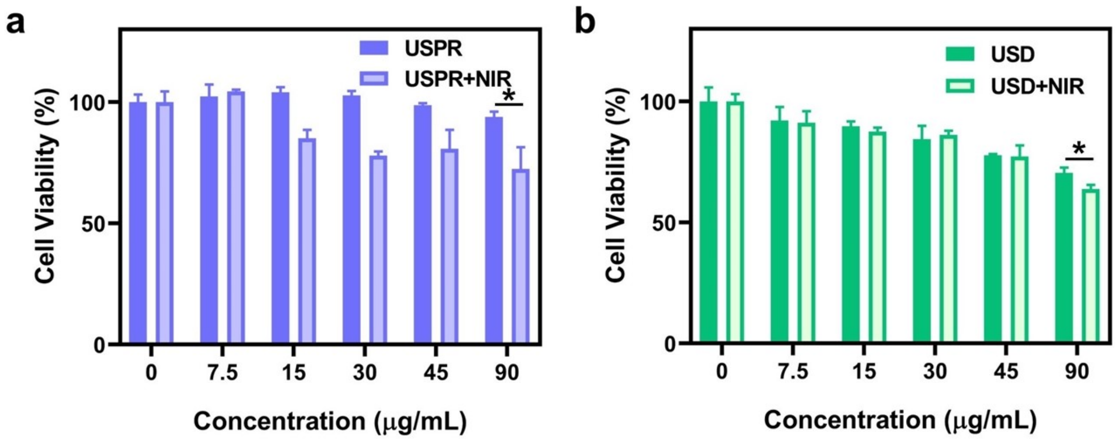

Figure S15. (a) Cell viabilities of MCF-7 cells treated with different concentrations of USPR or USPR+NIR for 24 h.(b) Cell viabilities of MCF-7 cells treated with different concentrations of USD or USD+NIR for 24 h. Data are the mean ± SD (n = 3).

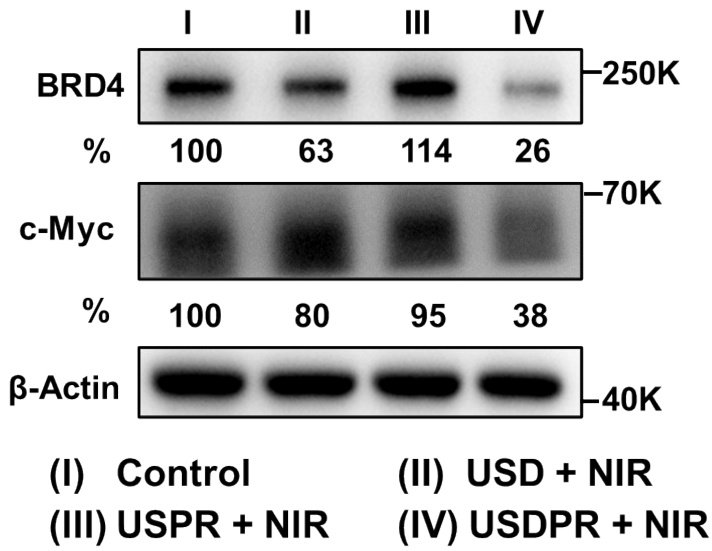

Figure S16. Western blot analysis of BRD4 and c-Myc levels in MCF-7 cells after different treatments. The concentration of USD, USPR, and USDPR is 90 μg/mL. The NIR irradiation time is 4 min (980 nm, 2 W/cm^2).

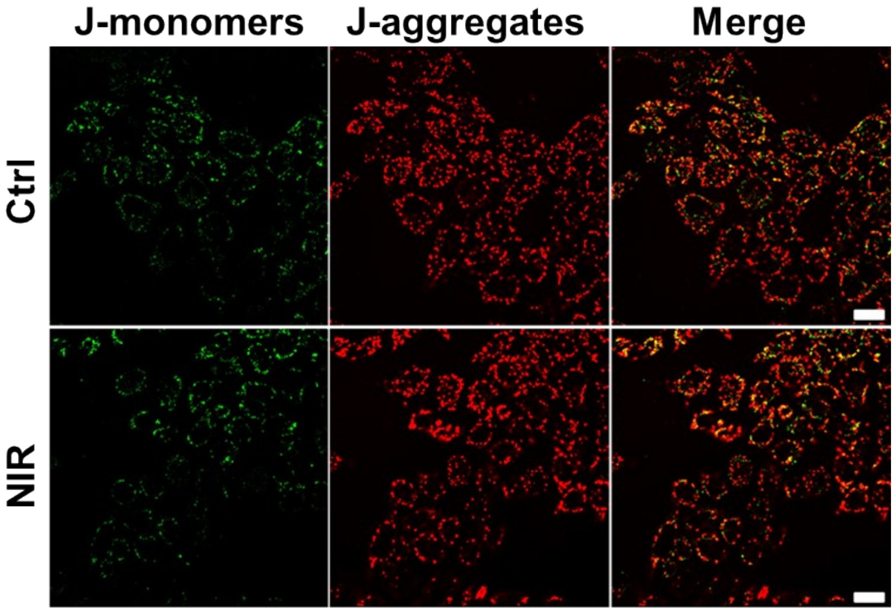

Figure S17. CLSM images of JC-1-stained MCF-7 cells without any treatments or only with 980 nm NIR irradiation for analysis of MMP. Scale bar: 20 μm.

Figure S18. *In vivo* fluorescence imaging of mice treated with USDPR and DCFH-DA before and after 4-min NIR light irradiation.

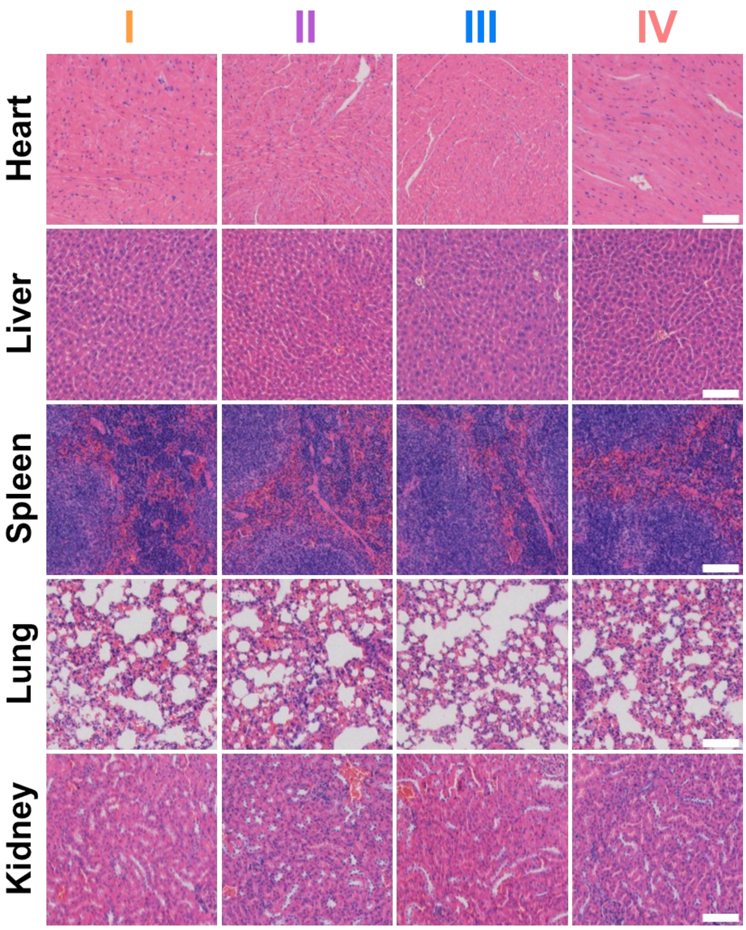

Figure S19. H&E staining images of major organs (heart, liver, spleen, lung, and kidney) of MCF-7 tumor-bearing nude mice from different treatment groups after 14 days of treatment. From I to IV: I, Saline; II, USPR+NIR; III, USDPR; IV, USDPR+NIR. Scale bar: 100 μm.

Section D: Uncropped full Western blot images

Figure 3a

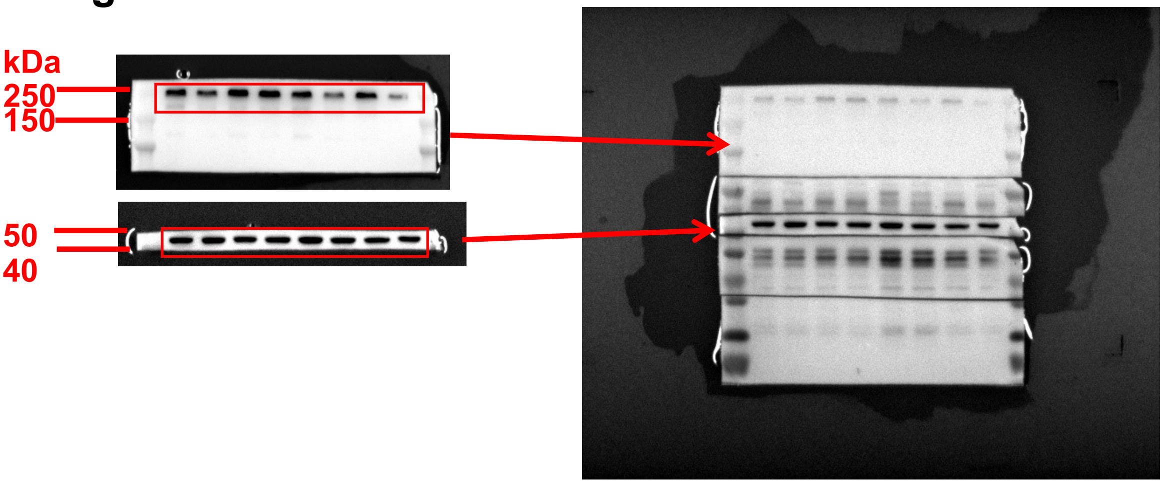

Uncropped full Western blot image of Fig. 3a. The samples derived from the same experiment, and the blots were processed in parallel. Loading controls, positive and negative controls, and molecular markers were all run on the same blot, with loading controls serving for normalization. The quantitation of protein expression represents relative protein level compared with the corresponding control after normalization with β-Actin (ImageJ software). The final western blotting images were obtained by overlaying the chemiluminescence image and the molecular weight markers image.

Figure 3b

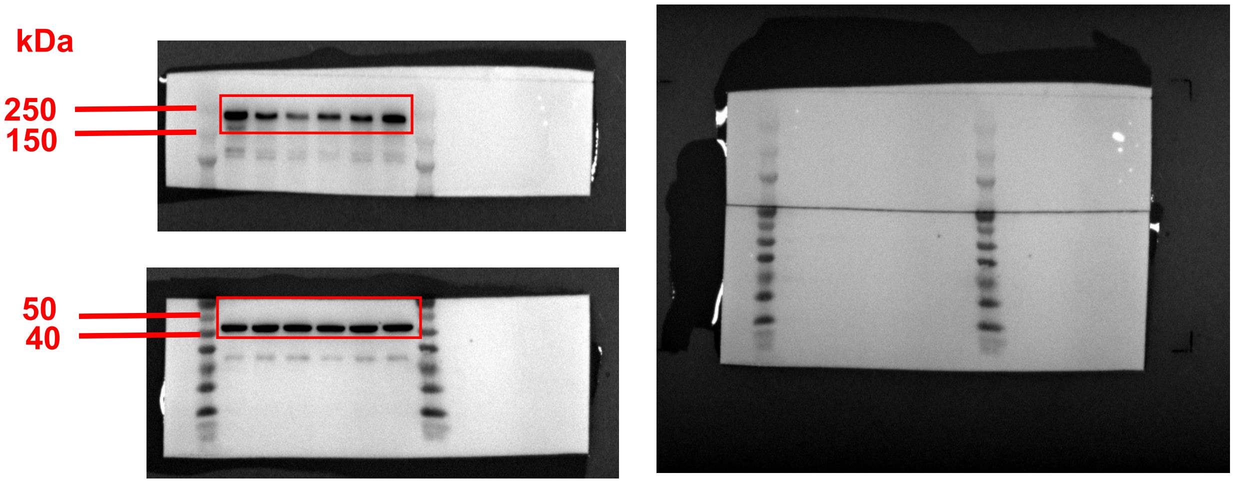

Uncropped full Western blot image of Fig. 3b. The samples derived from the same experiment, and the blots were processed in parallel. Loading controls, positive and negative controls, and molecular markers were all run on the same blot, with loading controls serving for normalization. The quantitation of protein expression represents relative protein level compared with the corresponding control after normalization with β-Actin (ImageJ software). The final western blotting images were obtained by overlaying the chemiluminescence image and the molecular weight markers image.

Figure 3c

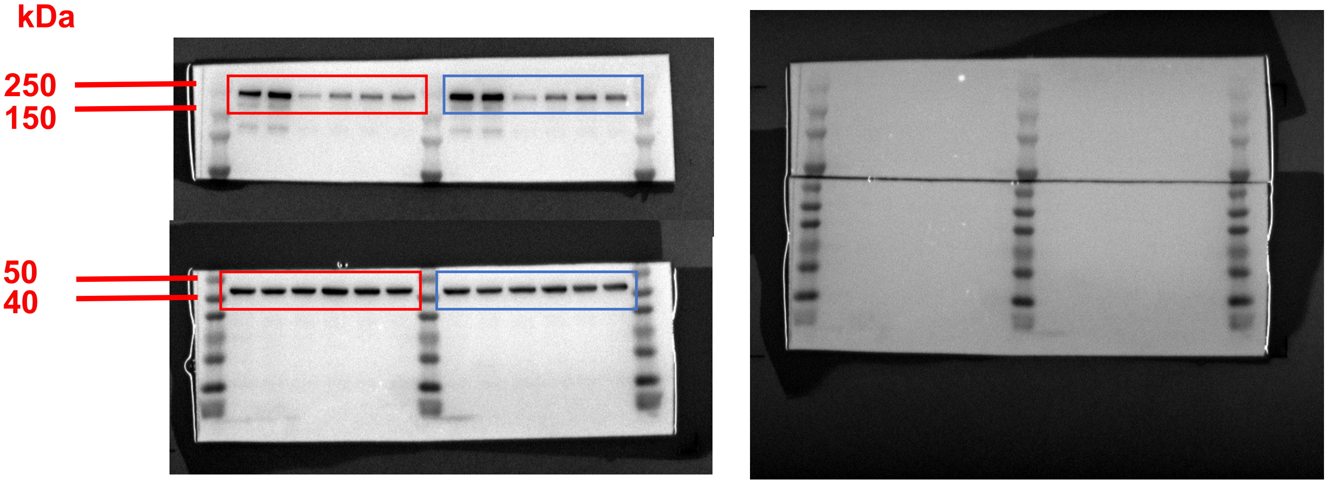

Uncropped full Western blot image of Fig. 3c. The samples derived from the same experiment, and the blots were processed in parallel. Loading controls, positive and negative controls, and molecular markers were all run on the same blot, with loading controls serving for normalization. The quantitation of protein expression represents relative protein level compared with the corresponding control after normalization with β-Actin (ImageJ software). The final western blotting images were obtained by overlaying the chemiluminescence image and the molecular weight markers image.

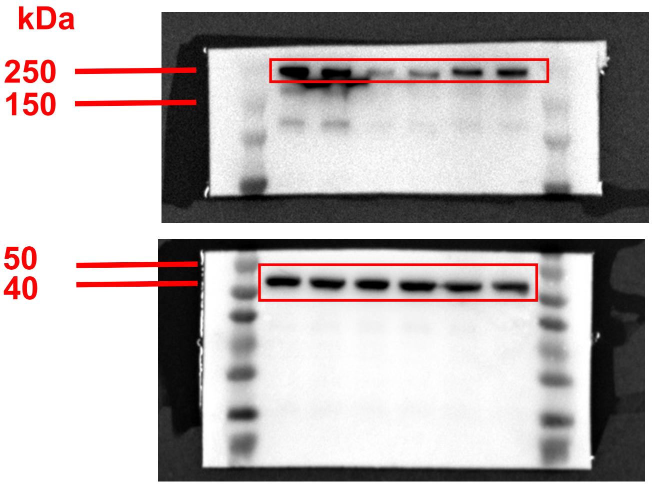

Uncropped full Western blot image of Fig. 3c. The samples derived from the same experiment, and the blots were processed in parallel. Loading controls, positive and negative controls, and molecular markers were all run on the same blot, with loading controls serving for normalization. The quantitation of protein expression represents relative protein level compared with the corresponding control after normalization with β-Actin (ImageJ software). The final western blotting images were obtained by overlaying the chemiluminescence image and the molecular weight markers image.

Figure 3d

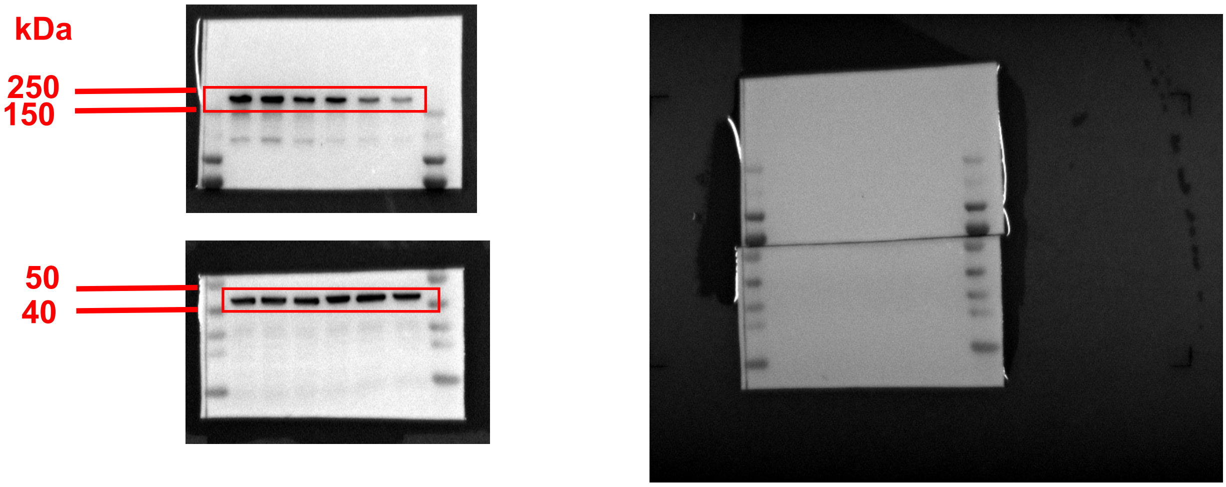

Uncropped full Western blot image of Fig. 3d. The samples derived from the same experiment, and the blots were processed in parallel. Loading controls, positive and negative controls, and molecular markers were all run on the same blot, with loading controls serving for normalization. The quantitation of protein expression represents relative protein level compared with the corresponding control after normalization with β-Actin (ImageJ software). The final western blotting images were obtained by overlaying the chemiluminescence image and the molecular weight markers image.

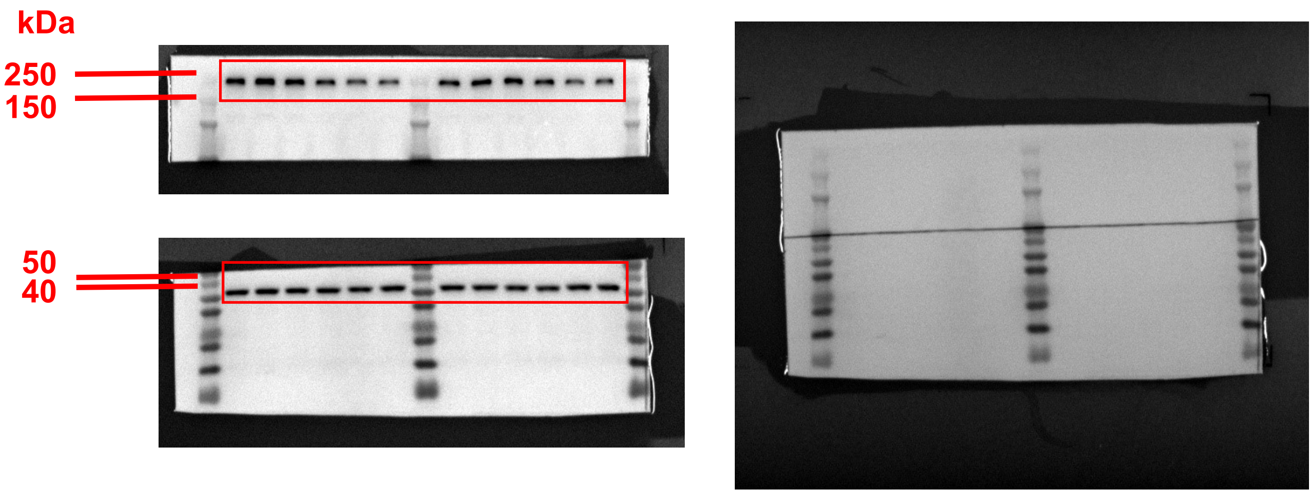

Uncropped full Western blot image of Fig. 3d. The samples derived from the same experiment, and the blots were processed in parallel. Loading controls, positive and negative controls, and molecular markers were all run on the same blot, with loading controls serving for normalization. The quantitation of protein expression represents relative protein level compared with the corresponding control after normalization with β-Actin (ImageJ software). The final western blotting images were obtained by overlaying the chemiluminescence image and the molecular weight markers image.

Figure 6f

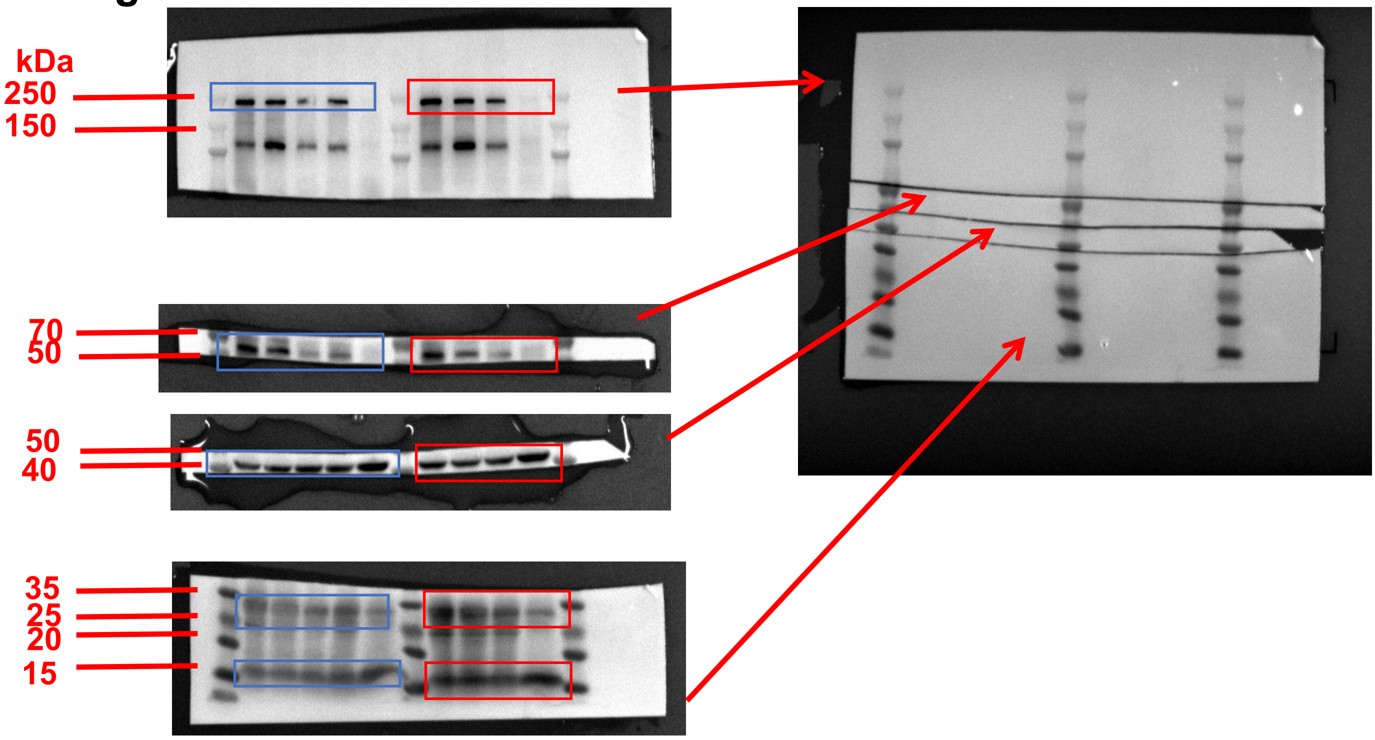

Uncropped full Western blot image of Fig. 6f. The samples derived from the same experiment, and the blots were processed in parallel. Loading controls, positive and negative controls, and molecular markers were all run on the same blot, with loading controls serving for normalization. The quantitation of protein expression represents relative protein level compared with the corresponding control after normalization with β-Actin (ImageJ software). The final western blotting images were obtained by overlaying the chemiluminescence image and the molecular weight markers image.

Figure S13

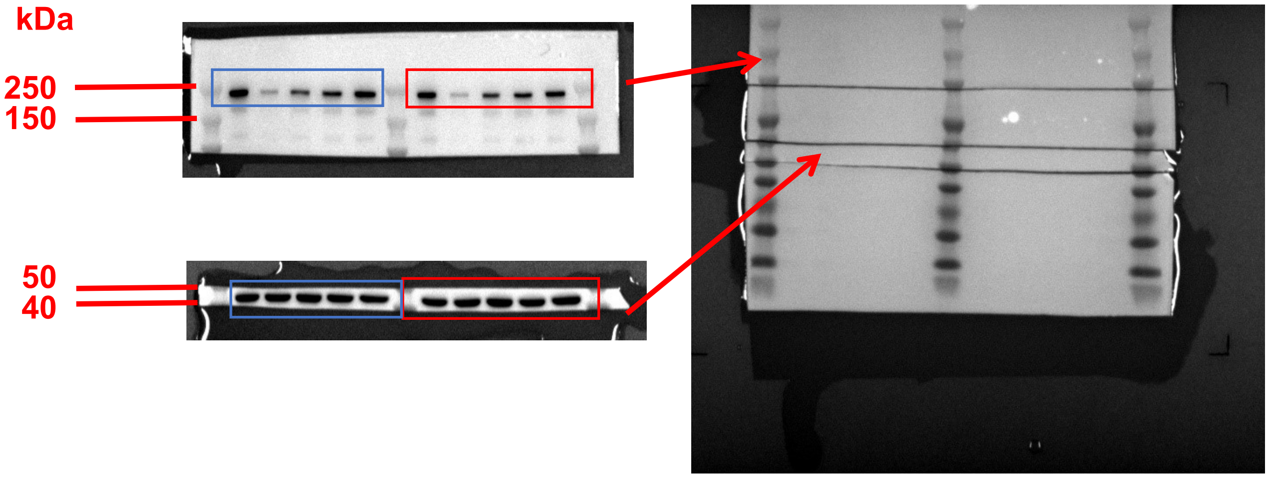

Uncropped full Western blot image of Fig. S13. The samples derived from the same experiment, and the blots were processed in parallel. Loading controls, positive and negative controls, and molecular markers were all run on the same blot, with loading controls serving for normalization. The quantitation of protein expression represents relative protein level compared with the corresponding control after normalization with β-Actin (ImageJ software). The final western blotting images were obtained by overlaying the chemiluminescence image and the molecular weight markers image.

Figure S16

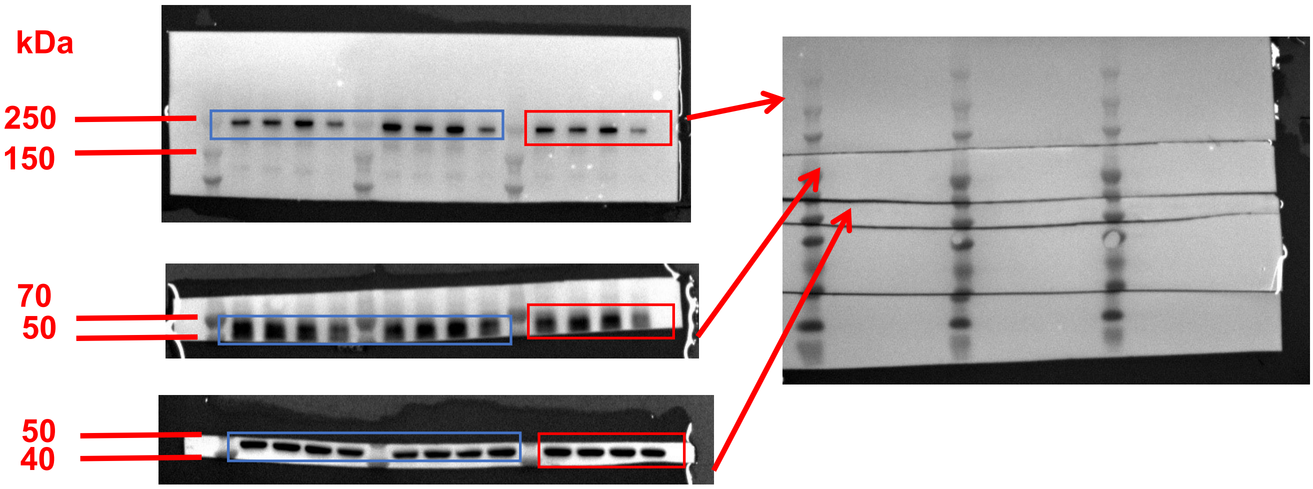

Uncropped full Western blot image of Fig. S16. The samples derived from the same experiment, and the blots were processed in parallel. Loading controls, positive and negative controls, and molecular markers were all run on the same blot, with loading controls serving for normalization. The quantitation of protein expression represents relative protein level compared with the corresponding control after normalization with β-Actin (ImageJ software). The final western blotting images were obtained by overlaying the chemiluminescence image and the molecular weight markers image.